Available online at www.sciencedirect.com

SciVerse ScienceDirect

journal homepage: www.elsevier.com/locate/he

SnO_2 functionalized AlGaN/GaN high electron mobility transistor for hydrogen sensing applications

Shao-Tsu Hung [a], Chi-Jung Chang [a,*], Chien-Hsing Hsu [a], Byung Hwan Chu [b], Chien Fong Lo [b], Chin-Ching Hsu [b], Stephen J. Pearton [c], Monta Raymond Holzworth [c], Patrick Guzek Whiting [c], Nicholas Guy Rudawski [c], Kevin S. Jones [c], Amir Dabiran [d], Peter Chow [d], Fan Ren [b]

[a] Feng Chia University, Department of Chemical Engineering, Taichung 40724, Taiwan
[b] University of Florida, Department of Chemical Engineering, Gainesville, FL 32611, USA
[c] University of Florida, Department of Materials Science and Engineering, Gainesville, FL 32611, USA
[d] SVT Associates, Eden Prairie, MN 55344, USA

ARTICLE INFO

Article history:
Received 2 December 2011
Received in revised form
22 March 2012
Accepted 23 March 2012
Available online 1 May 2012

Keywords:
Hydrogen sensor
High electron mobility transistors (HEMT)
Tin oxide (SnO_2)
Annealing

ABSTRACT

In this study, we report on a demonstration of hydrogen sensing at low temperature using SnO_2 functionalized AlGaN/GaN high electron mobility transistors (HEMT). The SnO_2 dispersion was synthesized via a hydrothermal method and selectively deposited on the gate region of a HEMT device through a photolithography process. The high electron sheet carrier concentration of nitride HEMTs provides an increased sensitivity relative to simple Schottky diodes fabricated on GaN layers. The morphology and crystalline properties of the SnO_2-gate, together with the texture of the multilayer films on the device were investigated by SEM, HRTEM, EDS and XRD. The effects of annealing treatment on the crystalline properties of the SnO_2-gate, and gas sensing properties of SnO_2-gated HEMT sensors were studied. The SnO_2-gated HEMT sensor showed fast and reversible hydrogen gas sensing response at low temperature.

1. Introduction

Hydrogen is a clean, renewable, and sustainable energy carrier for automotive fuel [1] and fuel cells [2] applications. There is great interest in detection of hydrogen sensors for the use in hydrogen-fueled automobiles and with proton-exchange membrane (PEM) and solid oxide fuel cells for spacecraft and other long-term sensing applications. However, hydrogen is a dangerous gas for storage and safety remains a top concern for applications of hydrogen energy. Hydrogen sensors need to be employed for monitoring leakage of hydrogen storage equipment and fuel tanks for spacecraft and hydrogen fuel cell automobiles. To reduce the power consumption, hydrogen sensors need, if possible, to be operated near room temperature without integrated on-chip heaters or if using a heater to increase the sensor sensitivity, it should consume minimal power. In addition, fast response time is also very important for many hydrogen detection applications [3].

AlGaN/GaN HEMTs show promising performance for use in broad-band power amplifiers in base station applications due to the high sheet carrier concentration, electron mobility in

* Corresponding author. Tel.: +886 4 24517250x3678; fax: 886 4 24510890.
E-mail address: changcj@fcu.edu.tw (C.-J. Chang).
0360-3199/$ – see front matter Copyright © 2012, Hydrogen Energy Publications, LLC. Published by Elsevier Ltd. All rights reserved.
doi:10.1016/j.ijhydene.2012.03.124

the two dimensional electron gas (2DEG) channel and high saturation velocity. The high electron sheet carrier concentration of nitride HEMTs is induced by piezoelectric and spontaneous polarization of the strained AlGaN layer. By modulating the current in the 2DEG channel of the HEMTs through a functionalized gate electrode, HEMT based sensors have been used to detect a variety of gases [4–7].

SnO_2 has been used for detecting CO and H_2 gases at different temperatures [8–10]. The gas sensing properties of the SnO_2-based gas sensors can be improved either by introducing dopants into the SnO_2 [11] or by changing the surface nanostructure of the SnO_2 [12,13] to enhance the sensitivity of the gas sensing. Hamaguchi et al. [14] reported the H_2 gas sensing properties of sensors prepared by fabricating tin oxide nanohole arrays on various electrodes. At 250 °C, the response time and the recovery time of the tin oxide nanohole arrays sensors were about 5 min. Both response and recovery times became much longer as the ambient temperature decreased.

In this work, the gas sensing properties of SnO_2-based sensors were improved neither by doping nor by using the SnO_2 with 1D or 2D nanostructure. A SnO_2 film was used as the gate electrode of HEMT sensor to detect 1% hydrogen at 50 °C.

2. Experimental

2.1. SnO_2-gated HEMT sensor

Fig. 1a shows a schematic cross-sectional view of the AlGaN/GaN HEMT device with SnO_2-gate. The Au-coated gate area was functionalized with SnO_2. The HEMT structure consists of a 2 μm GaN buffer layer, 25 nm $Al_{0.25}Ga_{0.75}N$ layer and 5 nm GaN cap layer. The epilayers were grown by molecular beam epitaxy (MBE) on sapphire substrates. A sheet carrier concentration of $\sim 10^{13}$ cm^{-2} and an electron mobility of 1200 $cm^2/V \cdot s$ were obtained at 300 K via Hall measurements. 50 × 50 μm^2 Ohmic contacts were composed of e-beam evaporated Ti/Al/Ni/Au and separated from each other by a 20 μm gap using the standard positive resist lift-off process. The Ohmic contacts were annealed at 850 °C for 45 s under flowing N_2. Then, a metal layer consisting of Ti/Au was deposited for interconnections.

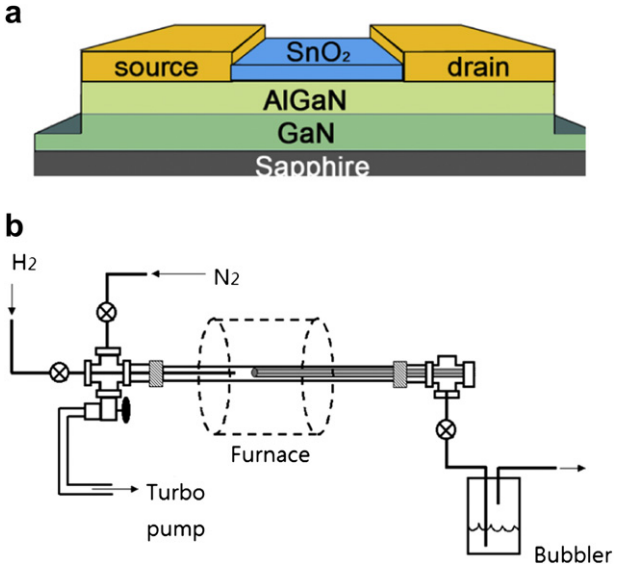

Fig. 1 – Schematic illustrations of (a) AlGaN/GaN HEMT sensor with SnO_2-gate (b) the hydrogen sensing system.

The gate area of the sensor was functionalized with a 20 nm of SnO_2 layer through a hydrothermally selective-area deposition method. The SnO_2 gel solution was prepared by adding 1 ml of HCl (40%) and 1 ml of NH_4OH (29%) in 100 ml of $SnCl_4$ aqueous solution. Then the solution was heated to 95 °C for 15 min. After being cooled to room temperature, the SnO_2 gel solution was spin-coated on the positive photoresist patterned HEMT sample with the gate area opened. To improve the adhesion, the sample was baked at 100 °C for 30 min prior to the standard resist lift-off process using acetone. Then the SnO_2-gated HEMT sample was annealed at 200 °C for 10 min to remove the residue solutions from the SnO_2. The SnO_2 functionalized gas sensor chip was mounted and wire bonded on a chip carrier for hydrogen detection.

2.2. Gas sensing

The system shown in Fig. 1b was utilized for gas sensing. The SnO_2 HEMT gas sensor was bonded to electrical feed-through and exposed to different gas ambients in the test chamber. Initially, the chamber was purged with pure nitrogen until the current reached a steady value. Then, 1% H_2 balanced with N_2 was introduced into the test system. The drain current of the SnO_2-gated HEMT gas sensor was monitored with an HP 4145B parameter analyzer. The temperature of the gas chamber was controlled by the furnace. The drain current for the SnO_2 HEMT gas sensor in nitrogen (I_0) and in the hydrogen-containing environment (I_{gas}) were measured during exposure to on–off cycles, which include sequential introduction of dilute H_2 in N_2 ("on") and dry N_2 ("off"). The gas sensitivity was determined using the following equation:

$$\text{Sensitivity}(\%) = \frac{I_{gas} - I_0}{I_0} \times 100\% \quad (1)$$

2.3. Characterization

The high resolution transmission electron microscope (HRTEM) experiments were carried out on a Transmission Electron Microscope (JEOL 2010F). The top-view images of films were observed by a HITACHI S4800 cold field emission scanning electron microscope and energy dispersive spectrometer. XRD studies were carried out with a MAC SCIENCE MXP3 diffractometer.

2.4. Crack analysis

Surface crack density of the SnO_2-gate region was measured before and after annealing using Image J (freeware available from the National Institute of Health at rsbweb.nih.gov/ij/). The length of each crack was approximated with a series of straight lines. The total crack length was normalized against the length of the scale bar in order to convert to a crack length in nanometers rather than pixels. The crack density was computed by taking the number of cracks observed on each

electrode and dividing by the electrode area, determined with a rectangular approximation. This area was normalized against the scale bar size in order to determine the density with respect to the area in 1 cm^2 rather than a number of pixels.

3. Results and discussion

3.1. Morphology and surface crack density

Fig. 2 illustrates a comparison between the surface morphology of the unannealed and annealed SnO_2-gated devices using plan view SEM images. Comparing the surface morphology of the SnO_2-gate region between the two samples, the annealed sample contains more surface cracks than the unannealed sample. Additionally, the surface crack density of the SnO_2-gate region of the samples was measured using Image J and found to be $4.1 \pm 1.4 \times 10^6$ cm^{-2} for the unannealed devices and $11.3 \pm 4.1 \times 10^6$ cm^{-2} for the annealed devices. Such an increase in surface crack density increased the surface area for the gas reaction and diffusion to enhance the gas sensing sensitivity.

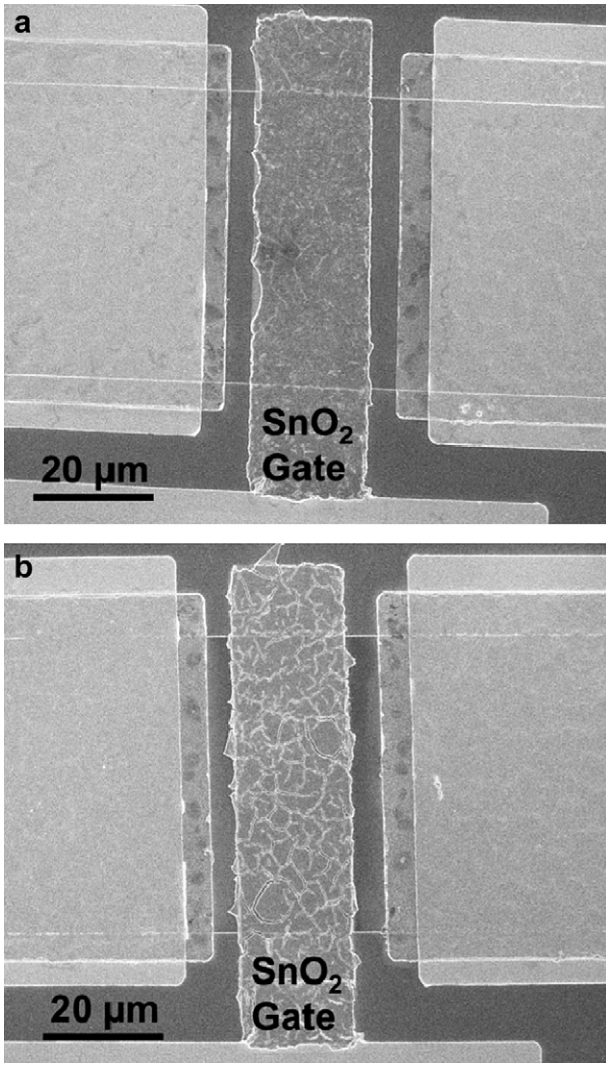

Fig. 2 – SEM images of the surface of the (a) unannealed (b) annealed device.

3.2. Cross-sectional structure

Fig. 3(a) shows the high resolution TEM image of the cross-sectional image of a SnO_2-gate HEMT device showing the SnO_2-gate and AlGaN epilayer. The selected area diffraction (SAD) pattern of SnO_2-gate is shown in the upper right corner of Fig. 3(a). The SnO_2-gate appears to be polycrystalline. It shows a discontinuous ring pattern arising from nanocrystallite structures. Fig 3(b) also includes scanning energy dispersive x-ray (EDS) analyses for different layers of the SnO_2-gated HEMT sensor chip. The upper layer consists of Sn and O elements. There is Al element in the middle layer. The Ga element appears in both the middle and the bottom layers. It confirmed sharp interfaces among SnO_2, AlGaN and GaN multilayer structures of the SnO_2-gated HEMT sensor chip and no intermixing of the layer occurred during the annealing step.

3.3. X-ray analysis

SnO_2 films were coated on the glass and annealed at various temperatures. XRD patterns of these films were investigated to check their crystalline structures. Fig. 4 shows XRD patterns of tin oxide film on glass substrate after being annealed at different temperature (200 °C, 300 °C and 400 °C). The XRD pattern revealed the formation of tetragonal rutile phase in annealed SnO_2 films. The peaks at 2θ values of 38.26° and 78.40° attributed to the (200) and (321) lattice plane reflections of SnO_2 tetragonal rutile crystal, respectively.

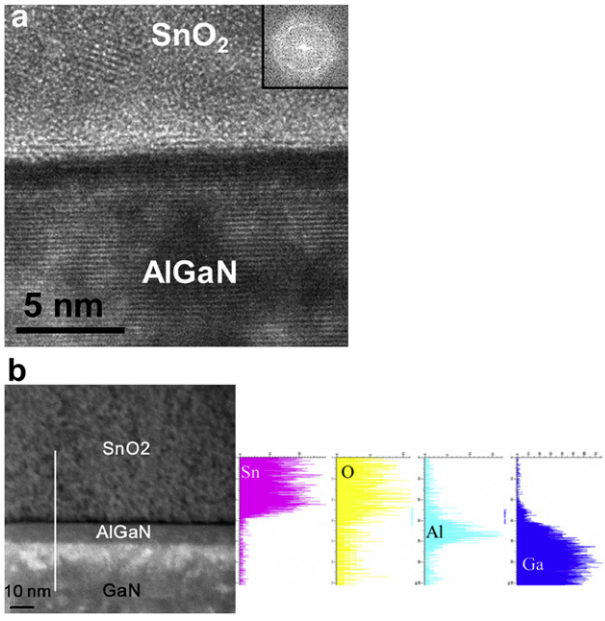

Fig. 3 – (a) High resolution TEM image of the cross section of a device showing the SnO_2-gate and AlGaN epilayer (inset diffraction pattern is from the SnO_2-gate and indicates that it is polycrystalline). (b) EDS analysis with cross-sectional SnO_2-gated HEMT sensor chip for different layer.

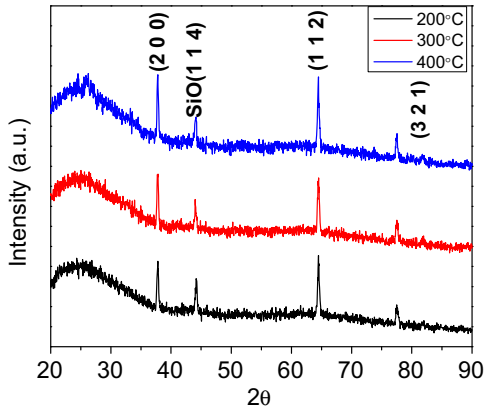

Fig. 4 – XRD patterns of tin oxide films annealed at different temperature (a) 200 °C (b) 300 °C and (c) 400 °C.

The average crystallite size (D) of tin oxide thin film was estimated using the Scherrer equation as follows [15]:

$$d = \frac{K\lambda}{\beta\cos\theta} \quad (2)$$

where d is the mean crystallite size, K is a grain shape dependent constant (0.9), λ is the wavelength of the incident beam, θ is a Bragg reflection angle and β is the full width half maximum.

The d values of different lattice plane reflections treated at various annealing temperatures are listed in Table 1. As the annealing temperature increased, the sharpness and intensity of the (200) and (321) peaks increased because of the crystalline growth. The average crystallite size was estimated from XRD measurements by the Scherrer equation. The crystallite size was increased slightly from 1.3 nm to 4.2 nm for (200) orientation as the annealing temperature increasing from 200 °C to 400 °C. The crystallite size was increased slightly from 3.1 nm to 5.1 nm for (321) orientation as the annealing temperature increasing from 200 °C to 400 °C. There was a tendency that the crystallite size decreased slightly from 7.8 to 3.7 nm for (112) orientation as the annealing temperature increased from 200 °C to 400 °C.

3.4. *Gas sensing properties*

3.4.1. *Sensing at low temperature*

The sensor functionalized with an unannealed SnO_2-gate electrode was not sensitive to the hydrogen. Once the SnO_2 was annealed, the sensors showed different degrees of sensitivity to the 1% H_2 ambient. Fig. 5 shows the time dependence measurements of the hydrogen sensing sensitivity conducted at 50 °C for SnO_2-gated HEMT sensors annealed at different temperatures during the sensor fabrication. The gas ambient was switched between 1% H_2 (in N_2) and pure N_2.The sensitivity for the sensor annealed at 200 °C showed large fluctuations upon the introduction and removal of H_2 gas (Fig. 5a). The signal to noise ratio was poor. Meanwhile, considerable changes in sensitivity were observed when the on and off responses toward H_2 were repeated 2 times. On the contrary, the sensitivity of the sensor annealed at 300 °C increased three times as

Table 1 – Average crystallite size of SnO_2 annealed at different temperature calculated from different diffraction peaks.

Orientation (hkl)	Annealing temperature		
	200 °C	300 °C	400 °C
(200)	1.3 nm	3.1 nm	4.2 nm
(112)	7.8 nm	3.5 nm	3.7 nm
(321)	3.1 nm	5.1 nm	5.1 nm

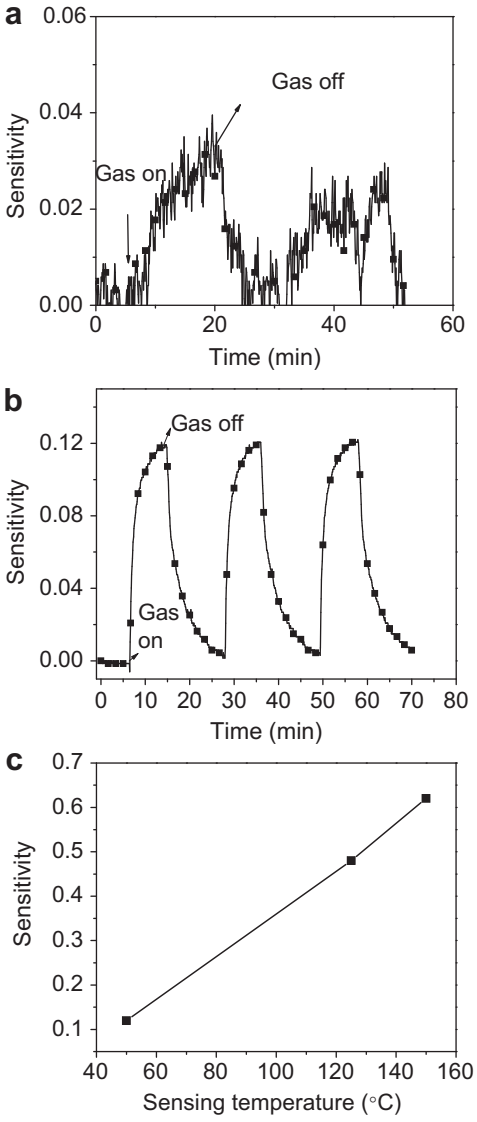

Fig. 5 – Time dependence measurements of the hydrogen detection sensitivity conducted at 50 °C for SnO_2-gated HEMT sensors with SnO_2 annealed at (a) 200 °C (b) 300 °C during the sensor fabrication. The surrounding gas was switched between 1% H_2 in N_2 (gas on) and pure N_2 (gas off). (c) The sensitivity at different sensing temperatures for SnO_2-gated HEMT sensors annealed at 300 °C.

compared to the sensor annealed at 200 °C (Fig. 5b). The response and the recovery times at 50 °C for SnO_2-gated HEMT sensor annealed at 300 °C are 4min and 9.5 min, respectively and the response and the recovery time were defined as the time for a sensor to reach 90% of the stable value. The sensor annealed at 300 °C showed no degradation with repeated exposure to hydrogen/nitrogen ambients. The better sensitivity of the sensor annealed at 300 °C was due to an increase of SnO_2 surface contact area, which was consistent with Liu's results in increasing porosity of the SnO_2 layer after annealing [16]. The good sensitivity and reversibility for the SnO_2-gated HEMT sensors annealed at 300 °C were attributed to the larger surface cracks and smaller grain size associated with the high temperature annealing.

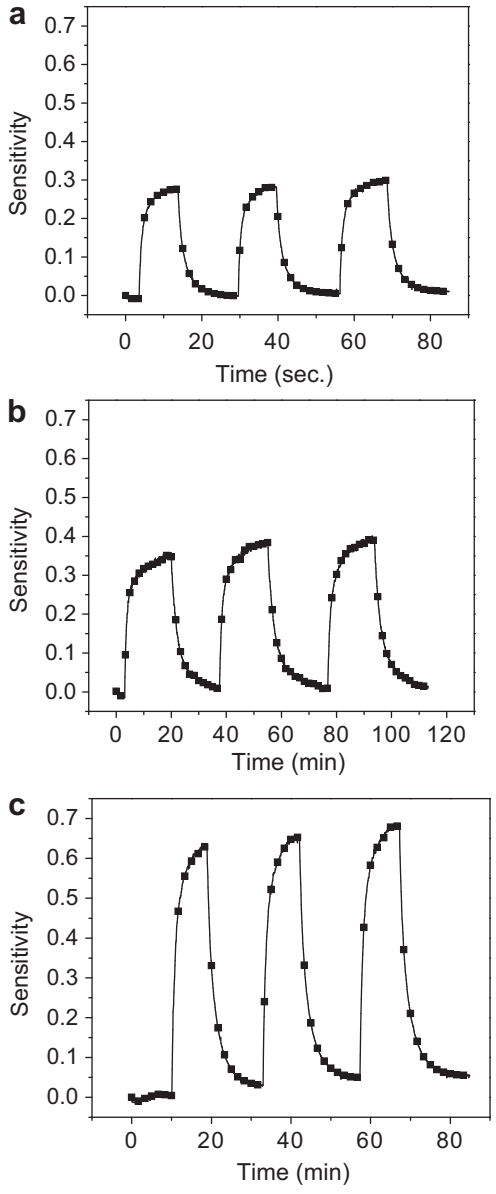

Fig. 6 – Time dependence of the sensitivity at 150 °C for SnO_2-gated HEMT sensors annealed at (a) 200 °C (b) 300 °C (c) 400 °C when the surrounding gas was switched between 1% H_2 in N_2 (gas on) and pure N_2 (gas off) for 3 cycles.

Table 1 shows the grain sizes of SnO_2 annealed at different temperatures based on different crystal orientations. All of them are either smaller or comparable to the space-charge length of SnO_2 (about 6 nm [12]). The small grains of SnO_2 allowed the sensors to be operated in the grain-controlled mode. Wang reported that the sensitivity could be exponentially enhanced when the grain size reduced to a scale comparable to the space-charge length [12]. The grain sizes of SnO_2 sensor annealed at 300 °C were smaller than 6 nm for all (200), (112) and (321) orientations. Sensors were operated in the grain-controlled mode. That may explain why the SnO_2-gated HEMT sensors annealed at 300 °C showed higher sensitivity and sharper response at 50 °C than the sensors annealed at 200 °C. To operate the sensors at 50 °C also helped to minimize the thermal-induced grain size changes to increase the stability and reliability of the sensor.

3.4.2. *Operating temperature and annealing temperature*

Fig. 5c shows the sensitivity of the SnO_2-gated gas sensor annealed at 300 °C operated at different temperatures. The sensitivity increased as the operating temperature in the testing chamber increased. For polycrystalline SnO_2, grain boundaries contributed most of the resistance and the surface resistivity of the oxide depended on the electron concentration near the surface. By increasing the ambient temperature, more free carriers were generated to reduce the resistivity, thus the sensitivity of the sensor increased. Similar trends were observed for the sensor annealed at 200, 300, and 400 °C. Fig. 6 illustrates the time dependence sensitivity measured at 150 °C for SnO_2-gated HEMT sensors annealed at 200, 300, and 400 °C during the sensor fabrication. When the gas sensing was conducted at 150 °C, all sensors exhibited improved sensitivity. For the sensor annealed at 200 °C, the sensitivity increased and large fluctuations observed for the testing conducted at 50 °C, as shown in Fig. 5(a), was not observed. Among them, the sensor annealed at 400 °C exhibited the highest sensitivity. The sensitivity almost doubled when the annealing temperature increased from 300 °C to 400 °C. Higher annealing temperature (>400 °C) may offer better crystallinity of the SnO_2. However, the Ohmic contact on the AlGaN/GaN would degrade.

4. Conclusion

Tin oxide thin films were fabricated as gates of the HEMT gas sensors and annealed at various temperatures. The annealing temperature exhibits large effect on the hydrogen gas sensing properties of the film. The annealing induced cracks and small grain size of the SnO_2-gate play an important role in the fast and reversible hydrogen gas sensing response at low temperature. After being annealed at a temperature higher than 300 °C, the crystallite sizes of the SnO_2-gate are smaller than the space-charge length of SnO_2 (about 6 nm). Sensors were operated in the grain-controlled mode. Based on the SEM images, the density of the crack is about 0.15/μm^2 for the annealed sample. We believe that the small crystallite should be the dominant contribution. Such rapid and reversible responses make the SnO_2-gated HEMT gas sensor suitable for practical applications in hydrogen sensing at low temperature.

Acknowledgments

The work at UF was partially supported by the Office of Naval Research (ONR) under contract number 00075094 monitored by Dr. Chagaan Baatar, NSF under contract number ECCS 0901711 monitored by Dr. Yogesh B. Gianchandani. The work at FCU was supported by the National Science Council (NSC) of Taiwan under contract number NSC 100-2628-E-035-003. The authors thank the assistance from the Precision Instrument Support Center of Feng Chia University.

REFERENCES

[1] Petkov T, Veziroglu TN, Sheffield JW. An outlook of hydrogen as an automotive fuel. Int J Hydrogen Energy 1989;14:449–74.
[2] Agnolucci P. Economics and market prospects of portable fuel cells. Int J Hydrogen Energy 2007;32:4319–28.
[3] Boon-Brett L, Black G, Moretto P, Bousek J. A comparison of test methods for the measurement of hydrogen sensor response and recovery times. Int J Hydrogen Energy 2010;35:7652–63.
[4] Travis A, Fan R, Stephen P, Byoung S-K, Wang H-T, Chih Y-C, et al. Advances in hydrogen, carbon dioxide, and hydrocarbon gas sensor technology using GaN and ZnO-based devices. Sensors 2009;9:4669–94.
[5] Wright JS, Wantae L, Norton DP, Pearton SJ, Ren F, Jason LJ, Ural Ant. Nitride and oxide semiconductor nanostructured hydrogen gas sensors. Semicond Sci Technol; 2010. 25:024002.
[6] Wang H-T, Kang B-S, Ren F, Fitch RC, Gillespie JK, Moser N, et al. Comparison of gate and drain current detection of hydrogen at room temperature with AlGaN/GaN high electron mobility transistors. Appl Phys Lett 2005;87: 172105–8.
[7] Wang Y-L, Chu BH, Chang CY, Lob CF, Peartona SJ, Dabiran A, et al. Long-term stability study of botulinum toxin detection with AlGaN/GaN high electron mobility transistor based sensors. Sensors and Actuators B 2010;146:349–52.
[8] Hubner M, Pavelko RG, Barsan N, Weimar U. Influence of oxygen backgrounds on hydrogen sensing with SnO_2 nanomaterials. Sensors and Actuators B 2011;154:264–9.
[9] Vuong DD, Sakai G, Shimanoe K, Yamazoe N. Preparation of grain size-controlled tin oxide sols by hydrothermal treatment for thin film sensor application. Sensors and Actuators B 2004;103:386–91.
[10] Pijolat C, Tournier G, Breuil P, Matarin D, Nivet P. Hydrogen detection on a cryogenic motor with a SnO_2 sensor network. Sensors and Actuators B 2002;82:166–75.
[11] Shukla S, Seal S, Ludwig L, Parish C. Nanocrystalline indium oxide-doped tin oxide thin film as low temperature hydrogen sensor. Sensors and Actuators B 2004;97:256–65.
[12] Wang Y, Jiang X, Xia Y. A solution-phase, precursor route to polycrystalline SnO_2 nanowires that can be used for gas sensing under ambient conditions. J Am Chem Soc 2003;125: 16176–7.
[13] Sxennik E, Colak Z, Kılınc N, Ozturk ZZ. Synthesis of highly-ordered TiO_2 nanotubes for a hydrogen sensor. Int J Hydrogen Energy 2010;35:4420–7.
[14] Hamaguchi T, Yabuki N, Uno M, Yamanaka S, Egashira M, Shimizu Y, et al. Synthesis and H_2 gas sensing properties of tin oxide nanohole arrays with various electrodes. Sensors and Actuators B 2006;113:852–6.
[15] Azaroff V. Elements of X-ray crystallography. New York: McGraw-Hill; 1968. p. 552.
[16] Liu X, Zhang D, Zhang Y, Dai X. Preparation and characterization of p-type semiconducting tin oxide thin film gas sensors. J Appl Phys 2010;107:064309–14.